Neural representations of observed interpersonal synchrony/asynchrony in the social perception network

Abbreviated title: Neural representations of synchrony

Maria Tsantani[1]*, Daniel Yon[1], Richard Cook[2]

[1]Department of Psychological Sciences,
Birkbeck, University of London, London WC1E 7HX, U.K.

[2]School of Psychology,
University of Leeds, Leeds LS2 9JU, U.K.

*Corresponding author: maria.tsantani[at]gmail.com

Conflict of interest

The authors declare no competing financial interests.

Acknowledgements

The research described in this article was funded by a Starting Grant awarded by the European Research Council to RC (ERC-2016-StG-715824).

Abstract

The visual perception of *individuals* is thought to be mediated by a network of regions in occipitotemporal cortex that supports specialized processing of faces, bodies, and actions. In comparison, we know relatively little about the neural mechanisms that support the perception of multiple individuals and the interactions between them. The present study sought to elucidate the visual processing of social interactions by identifying which regions of the social perception network represent interpersonal synchrony. In an fMRI study with 32 human participants (26 female, 6 male), we used multi-voxel pattern analysis to investigate whether activity in face-selective, body-selective, and interaction-sensitive regions across the social perception network supports decoding of synchronous vs. asynchronous head-nodding and head-shaking. Several regions were found to support significant decoding of synchrony/asynchrony, including extrastriate body area, face-selective and interaction-sensitive mid/posterior right superior temporal sulcus, and occipital face area. We also saw robust cross-classification across actions in extrastriate body area, suggestive of movement-invariant representations of synchrony/asynchrony. Exploratory whole-brain analyses also identified a region of right fusiform cortex that responded more strongly to synchronous than asynchronous motion. Critically, perceiving interpersonal synchrony/asynchrony requires the simultaneous extraction and integration of dynamic information from more than one person. Hence, the representations of synchrony/asynchrony cannot be attributed to augmented or additive processing of individual actors. Our findings therefore provide crucial new evidence that social interactions recruit dedicated visual processing within the social perception network that extends beyond any domain-specific processing engaged by the faces and bodies of individual agents.

Keywords:

Social interactions; Social perception; Interpersonal synchrony; Extrastriate body area; Superior temporal sulcus.

Significance statement

The presence of interpersonal synchrony is a critical cue when appraising the nature and content of social interactions from third-person perspectives. However, little is known about its representation within the human visual system. Here, we use fMRI to reveal distributed representations of interpersonal synchrony/asynchrony in several regions of the social perception network, notably extrastriate body area and superior temporal sulcus. There is great interest in whether the perception of social interaction engages specialized visual processing beyond any domain-specific processing recruited by the faces and bodies of the constituent individuals. Critically, perceiving interpersonal synchrony requires the simultaneous extraction and integration of dynamic information from more than one person. These results therefore provide key new evidence of dedicated interaction processing.

Introduction

The visual perception of *individuals* has been an active area of research for many years. This research tradition has revealed dedicated neural substrates for the visual processing of faces (Duchaine & Yovel, 2015; Haxby, Hoffman, & Gobbini, 2000), bodies (Peelen & Downing, 2007), and actions (Blake & Shiffrar, 2007). In comparison, we know relatively little about the neural mechanisms that support the perception of multiple individuals and the interactions between them. Over the last decade, however, studies using functional magnetic resonance imaging (fMRI) have consistently implicated two regions of the social perception network in the visual processing of social interactions.

Initial findings suggest that the extrastriate body area (EBA; Abassi & Papeo, 2020, 2022) and posterior superior temporal sulcus (pSTS; Kujala, Carlson, & Hari, 2012) show greater activation when participants view static images of face-to-face dyads, than when they view images of back-to-back dyads. Similar findings have been observed with dynamic stimuli; for example, authors have described stronger responses in EBA (Bellot, Abassi, & Papeo, 2021; Landsiedel, Daughters, Downing, & Koldewyn, 2022) and pSTS (Bellot et al., 2021; Centelles, Assaiante, Nazarian, Anton, & Schmitz, 2011; Isik, Koldewyn, Beeler, & Kanwisher, 2017; Landsiedel et al., 2022; Walbrin, Downing, & Koldewyn, 2018) when participants view interacting dyads (i.e., two actors shown facing each other, performing contingent, related actions), than non-interacting dyads (i.e., two actors shown non-facing and performing unrelated actions).

Neural representations in EBA and pSTS may encode information about the nature and content of social interactions. For example, stronger univariate responses are seen in both EBA and pSTS when participants view static images of semantically incongruous interactions, than when viewing images of congruous interactions (Quadflieg, Gentile, & Rossion, 2015). Having employed multi-voxel-pattern-analysis (MVPA), Walbrin and Koldewyn (2019) found that a classifier trained on pSTS and EBA responses was able to discriminate different types of social interaction (arguing vs. celebrating vs. laughing). The portion of pSTS sensitive to social interactions also discriminates different types of interactions between moving abstract shapes (Isik et al., 2017; Walbrin et al., 2018). For example, Isik et al. (2017) found that a classifier trained on responses in pSTS was able to discriminate animations depicting helping vs. hindering actions.

The present study sought to further elucidate the visual processing of social interactions by identifying which regions of the social perception network represent interpersonal synchrony.

Interpersonal synchrony refers to the temporospatial alignment of movements between interacting individuals that often occurs automatically, effortlessly, and unintentionally (Hoehl, Fairhurst, & Schirmer, 2021; Marsh, Richardson, & Schmidt, 2009). Perceived synchrony strongly influences our interpretation of dynamic social scenes. For example, dyads moving in synchrony are more likely to be perceived as a social unit than those moving asynchronously (Lakens, 2010; Lakens & Stel, 2011), and synchrony affords attributions of rapport (Lakens & Stel, 2011; Miles, Nind, & Macrae, 2009) and affiliation (Latif, Barbosa, Vatiokiotis-Bateson, Castelhano, & Munhall, 2014). At present, however, little is known about the neural representation of interpersonal synchrony within the visual system (Cracco et al., 2022).

We used MVPA to investigate whether activity in face-selective, body-selective, and interaction-sensitive regions across the social perception network supports decoding of synchronous vs. asynchronous head movements. We manipulated the presence of interpersonal synchrony between the actors, whilst holding the basic dyadic arrangement (i.e., face-to-face) constant. We predicted that responses in EBA and pSTS, which have been consistently implicated in the visual processing of social interactions (Abassi & Papeo, 2020, 2022; Bellot et al., 2021; Centelles et al., 2011; Isik et al., 2017; Kujala et al., 2012; Walbrin et al., 2018; Walbrin & Koldewyn, 2019), would be sensitive to interpersonal synchrony.

Materials and Methods

Participants

Thirty-three healthy right-handed adults aged 18-50 participated in the study. Our sample size was based on similar fMRI studies within the field (e.g., Abassi & Papeo, 2022). Participants reported normal or corrected-to-normal vision. One participant was excluded because of an incomplete dataset. The final sample consisted of 32 participants (26 female, 6 male) with a mean age of 27.66 years (*SD* = 6.93, range = 18-43). The study was approved by the relevant ethics committees of Birkbeck, University of London, and University College London. All participants provided written informed consent.

Stimuli

The video stimuli featured a pair of avatar heads (one male, one female) that moved synchronously or asynchronously relative to each other. Each three-dimensional model head was generated and rendered in Poser Pro 11.2 (Bondware, Inc., Murfreesboro, USA). The two heads were shown in profile view facing each other (Figure 1b). For each model, we

created a sequence of 40 images showing the head progressively moving forward and back ('nodding') and a sequence of 40 images showing the head progressively rotating from left to right ('shaking'). The images were used to create two types of synchronous videos featuring 0° (in-phase synchrony) and 180° (anti-phase synchrony) relative-phase offsets, and two types of asynchronous videos featuring 90° and 270° relative-phase offsets (Figure 1a).

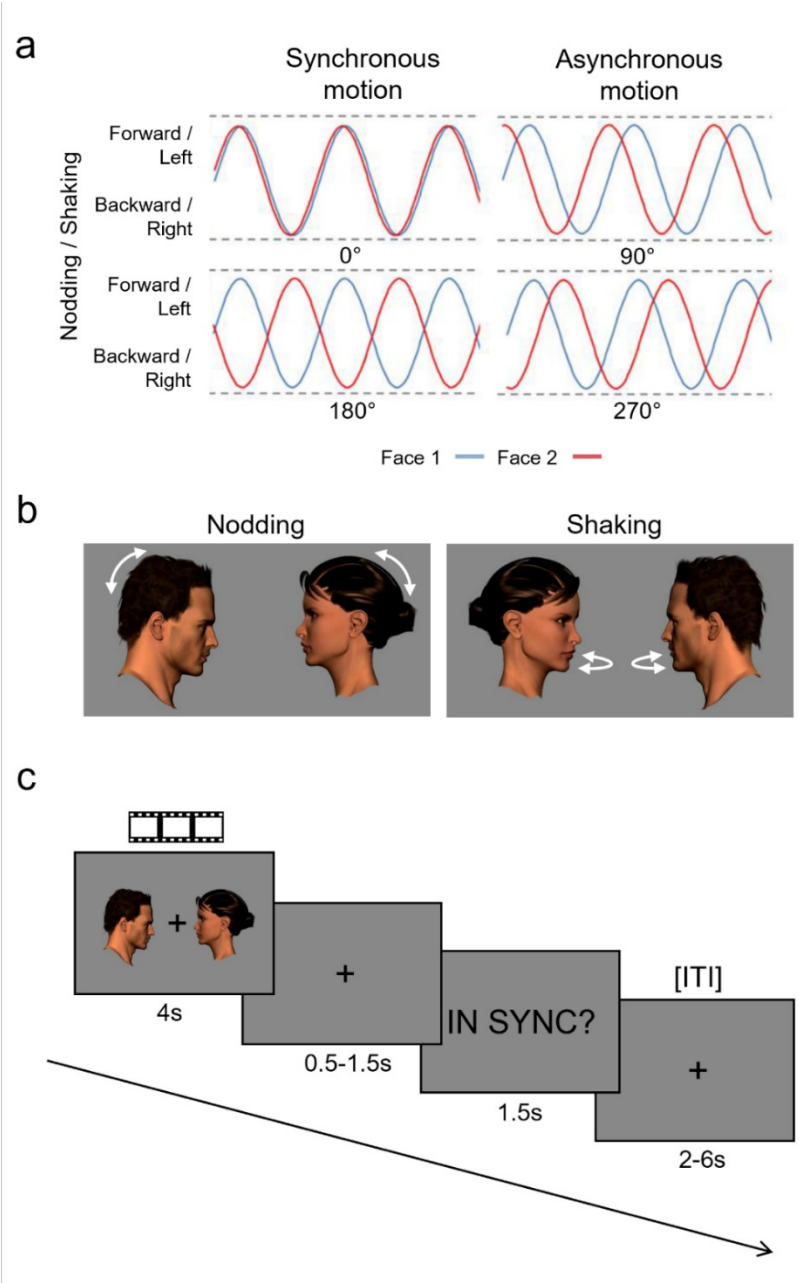

Figure 1. (a) The relative-phase relationships between Face 1 and Face 2 in synchronous stimulus videos (0° and 180° phase offset) and asynchronous stimulus videos (90° and 270° phase offset). (b) Illustration of nodding and shaking movements in the stimulus videos. (c) An example trial of the main experiment (stimulus images and text are magnified for illustration purposes). After viewing each video, participants responded with Yes/No button presses to the question 'in sync?' or 'out of sync?'. ITI: inter-trial-interval.

The order of the images for the head on the left was always the same, whereas the starting point in the sequence of images for the head on the right was modified to create the different phase offset conditions. For 0° phase offset, the movement of the two heads was mirrored. For 180° phase offset, the position of the heads was at opposite points of the movement cycle (e.g., in the nodding stimuli, one head would move forwards while the other moved backwards). For 90° phase offset, the right head led the left head by 1/4 of a cycle, and for the 270° phase offset, the right head led the left head by 3/4 of a cycle.

Videos of nodding and shaking movements were compiled using MATLAB (version R2019b). To avoid movement cycles time-locking to the TR of the MRI scanner, we made two sets of videos with different frame rates (28fps and 32fps). All videos were 4 seconds long. The 28fps videos depicted 2.8 cycles and the 32fps videos depicted 3.2 cycles. Two versions of each stimulus were produced, one with the female head on the left, one with the female head on the right. In total, there were 32 video stimuli: 2 movement types (nodding, shaking) × 4 phase offsets (0°,180°,90°,270°) × 2 frame rates (28fps, 32fps) × 2 model configurations (female left, female right).

MRI data acquisition

Participants were scanned using a 3.0 Tesla Siemens Prisma MRI scanner with a 32-channel head coil. Scanning took place at the Birkbeck-UCL Centre for Neuroimaging. We acquired whole-brain T1-weighted anatomic scans using MPRAGE (1.0 mm isotropic; 208 sagittal interleaved slices; PAT, factor 2; PAT mode, GRAPPA; TR, 2300ms; TE, 2.98ms; flip angle, 9°; matrix, 256 x 256; FOV, 256 mm). For the functional runs, we acquired T2*-weighted functional scans using EPI [3.0 mm isotropic; PAT, factor 2; PAT mode, GRAPPA; 34 ascending sequential slices; TR, 2000ms; TE, 30ms; flip angle, 78°; matrix, 64x64; FOV, 192 mm]. Slices were positioned at an oblique angle to include the temporal, occipital, and frontal lobes, and as much of the parietal lobe as possible.

Experimental Design and Statistical Analysis

Design of main experiment

The experimental runs presented videos of pairs of heads moving synchronously or asynchronously in an event-related design. The experiment was presented using the Psychophysics Toolbox v3.0 (Brainard, 1997; Pelli, 1997) in MATLAB (version 2014a) and was projected to a screen (1920 x 1200 pixels, 28.8 x 18 cm, 60Hz) at the back of the scanner bore, which the participants viewed through a mirror attached to the head coil. Participants viewed the screen from a distance of approximately 55cm (± 3 cm), and were

instructed to keep their gaze focused on the central fixation cross for the duration of the experiment.

There were 32 trials in each run. Each video stimulus was presented once per run without repetition. Each trial began with a stimulus video (4 seconds), followed by a fixation screen with a jittered duration of between 0.5 - 1.5 seconds (averaging 1 second) (Figure 1c). Participants then viewed a response screen with the question 'in sync?' or 'out of sync?' and had 1.5 seconds to respond 'Yes' or 'No' using buttons on a hand-held button box. The response screen was followed by a jittered inter-trial-interval of between 2 and 6 seconds (averaging 4 seconds) featuring a fixation screen. A fixation cross was present in the centre of the display at all times except during the response screen. The stimuli were presented in a random order. The pairing of the stimuli with the two versions of the task question (in/out of sync) was pseudorandomised. The randomisation was constrained such that the 28fps and 32fps version of each stimulus appeared with a different question. At the end of the run participants received feedback on their task performance (proportion correct). To familiarise them with the experimental task, participants first performed a practice run in which they received feedback (correct/incorrect) after each trial. Participants completed 8 runs of the experiment lasting around 6 minutes each.

Functional localisers

We used a standard localiser for face- and body-selective regions that is described in detail in Pitcher, Dilks, Saxe, Triantafyllou, and Kanwisher (2011), with permission from the authors. In a blocked design, participants viewed videos of moving faces, moving body parts (excluding the face), and moving objects, while performing a one-back task. The 3-second videos were presented randomly in 18-second blocks. Participants completed 2 runs of 12 stimulus blocks (4 blocks per stimulus category), presented in a pseudorandom order that prevented the consecutive presentation of blocks featuring stimuli from the same category. Participants also viewed three 18-second fixation blocks situated at the start, middle, and end of each run. The duration of each run was 276 seconds (4.6 minutes). Across both runs participants viewed 8 blocks of faces, 8 blocks of bodies, and 8 blocks of objects. The face/body localiser was typically completed after the main experiment runs.

We used a social interaction region localiser (Isik et al., 2017; Walbrin et al., 2018) to identify the interaction-sensitive region of pSTS (STS-I), with permission from the authors. In a blocked design, participants passively viewed videos of moving point-light displays of two individuals who were either interacting or performing independent actions. Videos of varying lengths (between 3 and 8 seconds) were grouped together and presented in 16-second

blocks. Participants completed 2 runs consisting of 12 stimulus blocks (6 per condition) and three fixation blocks situated at the start, middle, and end of each run. The presentation of the stimulus blocks alternated between the two stimulus categories, and always began with an interactions block in run 1, and an independent actions block in run 2. The pre-defined stimulus groupings presented in each block were randomised across runs. The duration of each run was 246 seconds (4.1 minutes). Across both runs, participants viewed 12 blocks of interactions and 12 blocks of independent actions. The interactions localiser was typically completed after the face/body localiser.

Data preprocessing and modelling

Functional images were preprocessed and analysed used Statistical Parametric Mapping (SPM12; Wellcome Department of Imaging Science, London; www.fil.ion.ucl.ac.uk/spm) in MATLAB (version R2021a). The first five (for the main experiment runs) or three (for the functional localisers) EPI images in each run served as dummy scans, and were discarded before preprocessing to allow for T1-equilibration effects. Images within each brain volume were slice-time corrected using the middle slice as a reference, and were then realigned to correct for head movements using the first image as a reference. Functional images from the main experimental runs were not smoothed, whereas images from the localiser runs were smoothed with a 6 mm Gaussian kernel (full width at half maximum). The participants' structural image in native space was coregistered to the realigned mean functional image, and was segmented into gray matter, white matter, and cerebrospinal fluid, saving the forward and inverse deformation fields (used for transformations to MNI space from the subject's native space and vice versa).

Mass-univariate general linear models (GLMs) were fitted to data from the main experiment runs, from the face/body localiser, and from the interactions localiser separately. GLMs included a regressor for the time course of each experimental condition, and six nuisance regressors for estimated head motion parameters. For the main experiment runs, we also included the response screen as a regressor of no interest. Regressors modelled the BOLD response following the onset of the stimuli and were convolved with a canonical hemodynamic response function (HRF). We used a high-pass filter cut-off of 128 s and autoregressive AR (1) model to account for serial correlations. The GLM analyses produced beta images for each condition showing the associated signal change across each voxel in the brain.

Classification analyses

Classification analyses were performed using The Decoding Toolbox (TDT; Hebart, Görgen, & Haynes, 2015) in MATLAB (version R2021a) at the individual subject level. In each analysis, beta images associated with two conditions of interest were used as input to a linear Support Vector Machine (SVM) classifier (LIBSVM; Chang & Lin, 2011). For all analyses, each condition was represented by 8 beta images, one from each run. We used a leave-one-out cross-validation procedure, whereby the classifier was trained to discriminate the two conditions based on images from 7 runs, and the resulting linear discriminant function was tested on images from the remaining run, in 8 cross-validation folds. For each ROI, we obtained the average classification accuracy across all folds. To determine whether classification accuracy in a given ROI was significantly greater than chance, we subjected participant accuracies to a one-sample *t*-test. Near identical results were obtained using a permutation testing approach more suitable for inferences of information prevalence (Stelzer, Chen, & Turner, 2013).

In our main analysis we tested the decoding of synchronous vs. asynchronous movement collapsing across all other stimulus characteristics, including the type of head movement (nodding, shaking). To test whether representations of synchrony and asynchrony generalise across movement type, we performed a cross-classification analysis by training the classifier to distinguish synchronous from asynchronous shaking and testing it on nodding, and *vice versa*. The cross-classification analysis followed the same leave-one-out procedure described above. All reported *p*-values are two-tailed. For each analysis, correction for multiple comparisons across 10 ROIs was performed using the False Discovery Rate (FDR) with $q = .05$.

Exploratory whole-brain univariate analyses

For these analyses only, images from the main experiment runs were normalised to standard MNI space and smoothed with a 6-mm Gaussian kernel (full width at half maximum) to account for anatomical variability across subjects. The normalised and smoothed images were subjected to mass-univariate GLMs, and we defined the contrasts synchronous > asynchronous and asynchronous > synchronous. For group-level analysis, the contrast images were subjected to one-sample *t*-tests. The resulting *t*-contrast images were thresholded at $p < .001$ at the voxel level and corrected for multiple comparisons using FWE at $p < .05$ at the cluster level. We report clusters with 2 or more voxels, coordinates of peak voxels in MNI space and anatomical labels based on the Automated Anatomical Labelling atlas (Rolls, Huang, Lin, Feng, & Joliot, 2020).

Definition of functional ROIs

Subject-specific functional ROIs were defined using a group-constrained subject-specific method (Fedorenko, Hsieh, Nieto-Castañón, Whitfield-Gabrieli, & Kanwisher, 2010; Julian, Fedorenko, Webster, & Kanwisher, 2012), in which group-level parcels are used to constrain functionally-localised ROIs in individual subjects. This method has the benefit of reducing experimenter bias in the definition of ROIs while allowing for anatomical variability in ROI locations across participants. Group-level parcels of face-selective and body-selective regions were derived in Julian et al. (2012), who used the same face/body localiser as the present study, and were downloaded from http://web.mit.edu/bcs/nklab/GSS.shtml. There was no available group-level parcel for the interaction-sensitive STS region (STS-I), so we derived the parcel from a group analysis of interaction localiser data from our own participant sample. To conduct a group-level analysis for the contrast Interactions > Independent actions, we first normalised all scans to the standard MNI template and repeated the GLM analysis for each subject. First-level *t*-contrast images were then subjected to a second-level one-sample *t*-test. A parcel including the right posterior and mid STS was created from the continuous significant voxels around the peak voxel in the resulting second-level *t*-map, thresholded at $p < .001$ uncorrected.

All group-level parcels in standard MNI space were transformed to the native space of each individual subject using the inverse deformation fields obtained during the segmentation procedure. The images were resliced to the same resolution as the functional images and trimmed to remove any voxels that were not present in the participant's brain mask obtained from the relevant GLM analysis.

Using the data from the face/body localiser, we defined face-selective ROIs by intersecting *t*-contrast images for Faces > Objects with group-level parcels of the left and right FFA, OFA, and STS face region (STS-F). We defined body-selective ROIs by intersecting *t*-contrast images for Bodies > Objects with parcels of the left and right EBA. From the interactions localiser data, we defined the interaction-sensitive STS ROI (STS-I) by intersecting *t*-contrast images for Interactions > Independent actions with the group-level STS-I parcel.

For each subject, ROIs were defined as the most active 30% of voxels within each group parcel. ROIs with fewer than 30 voxels were discarded. Face-selective ROIs included the rFFA (28 participants, mean number of voxels = 55.07, range = 41-67), the rOFA (26 participants, mean vox. = 44.73, range = 33-60), the rSTS-F (all participants, mean vox. = 165.38, range = 129-208), and the lSTS-F (all participants, mean vox. = 55.17, range = 43-

70). The lFFA and lOFA could not be localised with at least 30 voxels in the majority of participants, and were therefore excluded from the analysis. Body-selective ROIs included the rEBA (all participants, mean vox. = 146.81, range = 115-185) and the lEBA (all participants, mean vox. = 136.13, range = 108-171). The STS-I was localised in all participants, and had an average size of 78.63 voxels (range 45-102). The STS ROIs covered the posterior part of the STS, extending to the mid STS in some participants. Due to a large number of overlapping voxels (*M* = 35.59, *SD* = 15.17, range = 7-63) between the STS-I and the larger rSTS-F ROI, we made an additional face-selective rSTS ROI that excluded all voxels that overlapped with the STS-I. This rSTS-F* ROI had an average size of 129.78 voxels (range = 98-178). The location of the various ROIs in an example participant is illustrated in Figure 2.

Definition of non-social comparison ROIs

The primary focus of our classification analyses was the social perception network. However, we also examined the distributed responses seen in two non-social comparison ROIs: V1 and the middle temporal area (MT). V1 was selected as a control region. Given that the low-level features of our synchronous and asynchronous stimuli were closely-matched, we reasoned that the distributed responses seen in V1 would be unlikely to support synchrony/asynchrony classification (see also Caplovitz, Barroso, Hsieh, & Tse, 2008). At the outset, we had no strong expectation about the ability of MT responses to support decoding of synchrony/asynchrony. However, MT is known to play a key role in visual motion processing (Born & Bradley, 2005; Kolster, Peeters, & Orban, 2010) and has been implicated in perceptual grouping based on motion cues (e.g., Ferber, Humphrey, & Vilis, 2003). Moreover, there is some suggestion that MT is sensitive to visual features of dyadic interactions (Landsiedel et al., 2022; Quadflieg et al., 2015).

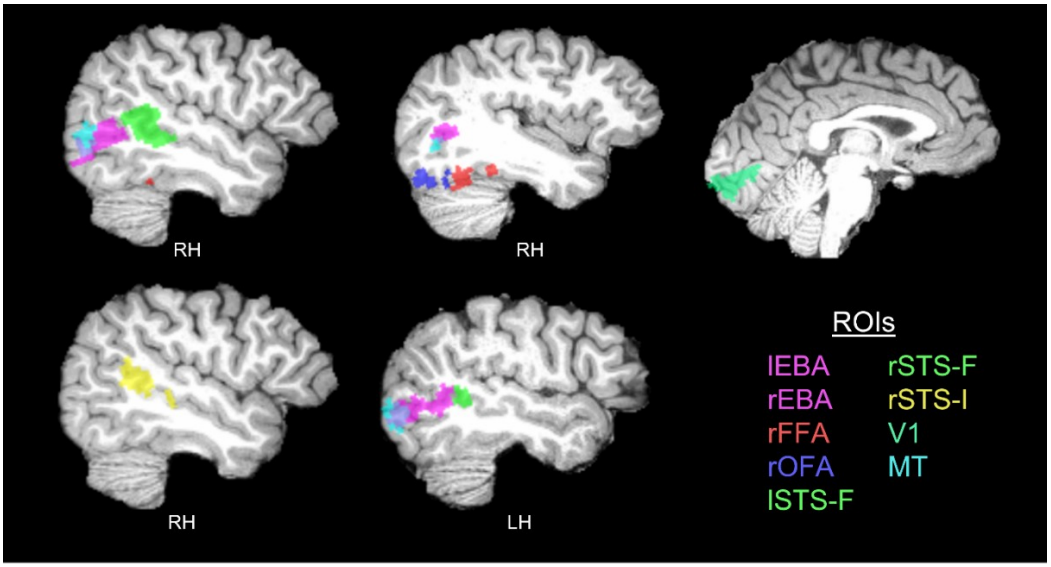

Figure 2. Location of ROIs in one example participant. RH: right hemisphere; LH: left hemisphere.

Probabilistic masks of V1 and MT were derived in Wang, Mruczek, Arcaro, and Kastner (2015) and downloaded from https://scholar.princeton.edu/napl/resources. Our V1 and MT masks were bilateral, and the V1 mask included ventral and dorsal subregions. Masks were transformed to each subject's native space in the same way as the functional ROIs (see above). Individual-subject V1 ROIs were defined as the 200 voxels with the highest probabilities. MT ROIs were defined as the 100 voxels with the highest probabilities.

Data and code accessibility

Beta images obtained from the GLMs, task accuracy scores, and MATLAB analysis scripts are available via the Open Science Framework (https://osf.io/s6phj/?view_only=ad89001d587b4cfda4a3b286ce023332).

Results

Task accuracy

Participants correctly identified the stimuli as synchronous or asynchronous on 89.59% of trials on average (*SD* = 9.63, range = 65.23-99.61). There were no differences in accuracy between synchronous (*M* = 91.04%, *SD* = 9.36) and asynchronous stimulus trials (*M* = 88.13%, *SD* = 12.84) [$t_{(31)}$ = 1.418, *p* = .166]. Accuracy was slightly higher for shaking (*M* = 90.82%, *SD* = 8.20) compared to nodding stimuli (*M* = 88.35%, *SD* = 11.71) [$t_{(31)}$ = 2.265, *p* = .031].

Decoding synchrony vs. asynchrony

We found above-chance decoding of synchronous vs. asynchronous movement in bilateral EBA, in rOFA, in face-selective and interaction-sensitive regions of rSTS (STS-F, STS-F*, STS-I), and in MT (Figure 3; Table 1). The same patterns were obtained using an alternative permutation testing approach (Stelzer et al., 2013), except the lSTS-F region was found to contain significant information after FDR correction for multiple comparisons. Classification accuracies were significantly lower in the V1 comparison region compared to lEBA [$t_{(31)}$ = 3.143, p = .004], rEBA [$t_{(31)}$ = 2.755, p = .010], and MT [$t_{(31)}$ = 3.040, p = .005]. The difference between accuracies in V1 and rSTS-F* did not survive FDR correction [$t_{(31)}$ = 2.111, p = .043], and no other differences were significant (all ps > .07). There were no significant pairwise differences in classification accuracy between regions that showed significant decoding of synchronous vs. asynchronous movement (all ps > .12).

In general, decoding of interpersonal synchrony was high in the MT comparison region, and decoding accuracy did not differ significantly between MT and the ROIs we believe to be part of a distinctive social perception network (all ps >.06). However, one potential reason for such high decoding of interpersonal synchrony in MT is that, across participants, this ROI contained several voxels that overlapped with EBA (lEBA overlap: M = 22.03, SD = 8.97, range = 3-35 voxels; rEBA overlap: M = 28.66, SD = 14.92, range = 5-58 voxels). With overlapping voxels removed, on average, MT size was reduced by around 50% to 49.31 voxels (range = 25-83), lEBA size was reduced by around 16% to 114.09 voxels (range = 92-154), and rEBA size was reduced by around 20% to 118.16 voxels (range = 73-162). When overlapping voxels were excluded from each ROI, decoding of interpersonal synchrony remained high in EBA [lEBA: M = 58.20%, $t_{(31)}$ = 3.824, p < .001; rEBA: M = 60.74%, $t_{(31)}$ = 5.016, p < .001]. However, decoding in MT dropped substantially to 53.52%, and was no longer significantly different from chance [$t_{(31)}$ = 1.579, p = .125].

Table 1. Mean classification accuracies for decoding of synchronous from asynchronous movement and one-sample *t*-test results. Asterisks indicate p-values that survived FDR correction.

ROI	Mean accuracy (%)	*Df*	*t*-statistic	*p*-value
lEBA	59.18	31	3.681	.001*
rEBA	58.40	31	3.876	.001*
rFFA	52.90	27	1.223	.232
rOFA	55.29	25	2.553	.017*
lSTS-F	55.42	29	2.120	.043
rSTS-F	56.05	31	3.350	.002*
rSTS-F*	58.01	31	4.067	< .001*
rSTS-I	55.47	31	2.763	.010*
V1	51.95	31	0.961	.344
MT	59.57	31	4.198	< .001*

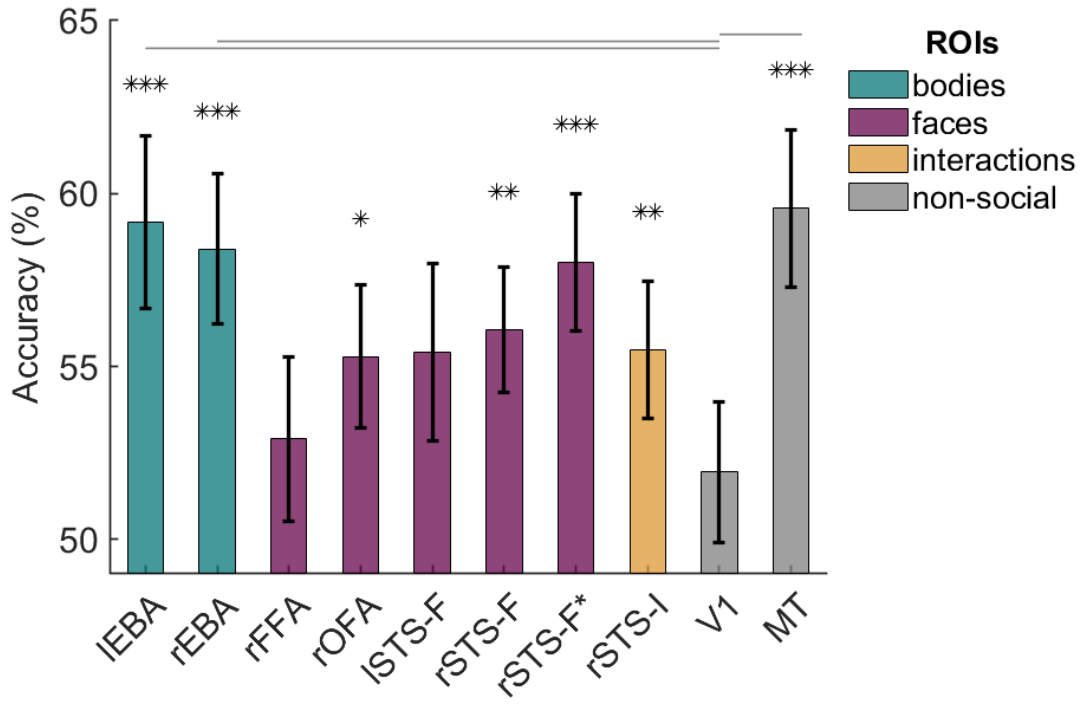

Figure 3. Mean classification accuracies for decoding of synchronous vs. asynchronous movement in body-selective ROIs (green), face-selective ROIs (purple), an interaction-sensitive ROI (yellow), and non-social comparison ROIs (grey). Error bars show standard error. Asterisks indicate above-chance accuracy after FDR correction for 10 comparisons: *$p \leq .05$; **$p \leq .01$, ***$p \leq .001$. Horizontal lines above bars indicate significant pairwise differences between each comparison ROIs and all other ROIs.

Generalisation across movement type

We tested whether representations of interpersonal synchrony generalise across nodding and shaking movement using cross-classification. We found significant above-chance cross-classification of synchronous vs. asynchronous movement across both directions (generalising from nodding to shaking, and from shaking to nodding) in lEBA [N→S: M = 55.47%, $t_{(31)} = 3.016$, $p = .005$; S→N: M = 57.42%, $t_{(31)} = 3.724$, $p = .001$], rEBA [N→S: M = 57.23%, $t_{(31)} = 4.016$, $p < .001$; S→N: M = 55.47%, $t_{(31)} = 2.634$, $p = .013$], and rFFA [N→S: M = 53.57%, $t_{(27)} = 2.458$, $p = .021$; S→N: M = 55.13%, $t_{(27)} = 3.256$, $p = .003$] (Figure 4). Generalisation from nodding to shaking (only) was found in the lSTS-F [M = 54.79%, $t_{(30)}$ = 2.419, $p = .022$] and in MT [M = 55.27%, $t_{(31)} = 3.044$, $p = .005$]. Cross-classification accuracies did not survive FDR correction in other ROIs (N→S: all Ms < 55%, all ps >.03; S→N all Ms < 55%, all ps >.03).

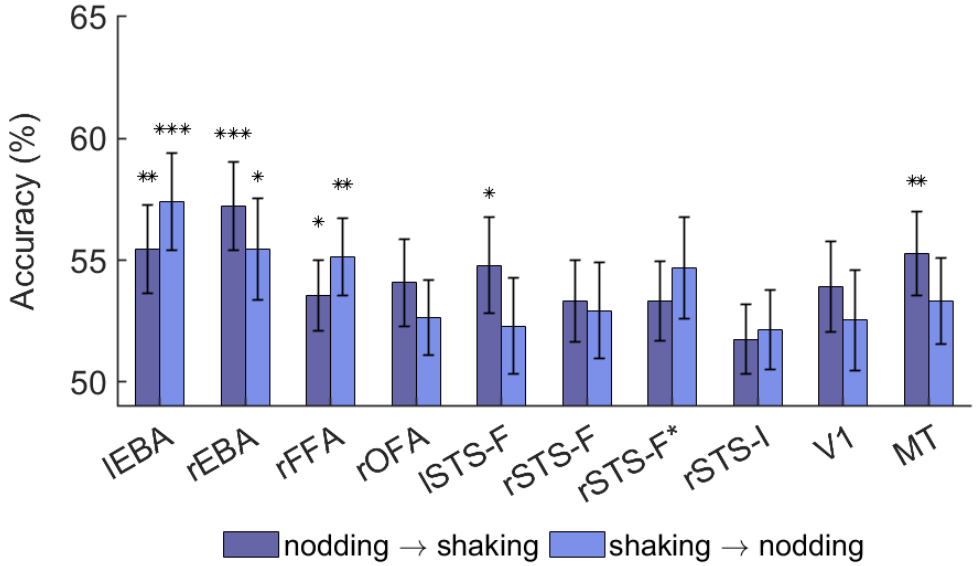

Figure 4. Mean cross-classification accuracies for decoding of synchronous from asynchronous movement with generalisation from nodding to shaking, and generalisation from shaking to nodding. Error bars show standard error. Asterisks indicate above-chance accuracy after FDR correction for 10 comparisons: *$p \leq .05$; **$p \leq .01$, ***$p \leq .001$.

Univariate analyses

To compare univariate responses to synchronous and asynchronous movement, for each ROI and each participant we calculated the mean beta value across all voxels included in the ROI, separately for synchronous and asynchronous stimuli (Figure 5). We found significantly greater responses to asynchronous stimuli compared to synchronous stimuli in rEBA [$t_{(31)} = 3.197$, $p = .003$] and lSTS [$t_{(29)} = 3.088$, $p = .004$]. Comparisons in other ROIs did not survive FDR correction ($p > .02$).

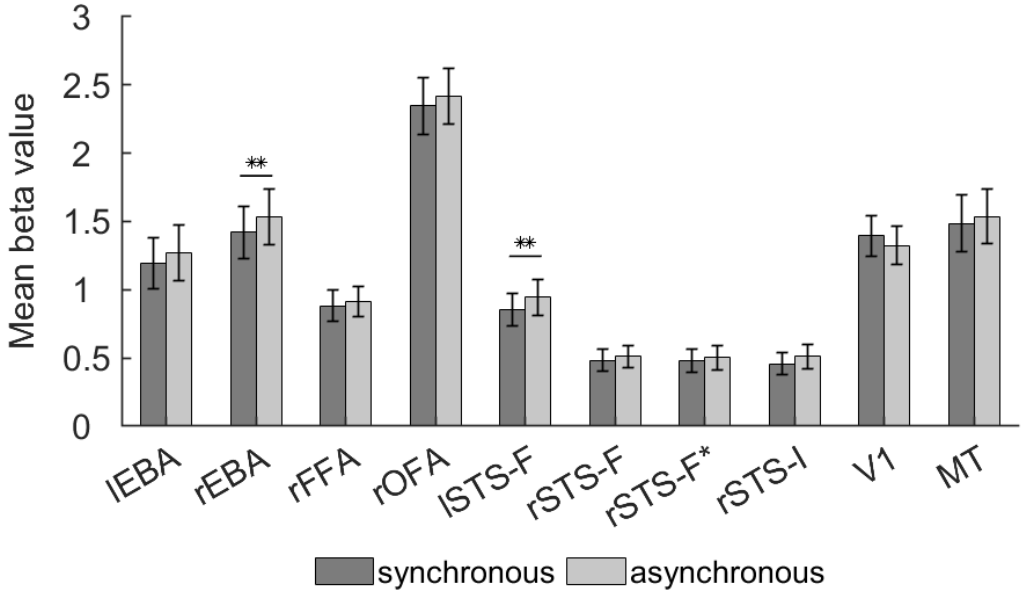

Figure 5. Mean beta values for synchronous and asynchronous movement in each ROI. Error bars show standard error. Asterisks indicate above-chance accuracy after FDR correction for 10 comparisons: **$p \leq .01$.

We also performed exploratory whole-brain univariate analyses to test for regions showing greater responses to synchronous than asynchronous motion, and *vice versa*.
The contrast synchronous > asynchronous revealed a small cluster with a peak in the right fusiform gyrus (k = 7, x = 30, y = -40, z = -13, t = 7.020, p < .001). The contrast asynchronous > synchronous revealed 3 clusters with peaks in the left supplementary motor area (k = 65, x = -3, y = 17, z = 44, t = 8.874, p < .001), left precentral gyrus (k = 7, x = -40, y = 2, z = 39, t = 6.591, p < .001) and within the right frontal lobe (peak region undefined) (k = 6, x = 32, y = -1, z = 46, t = 6.601, p < .001).

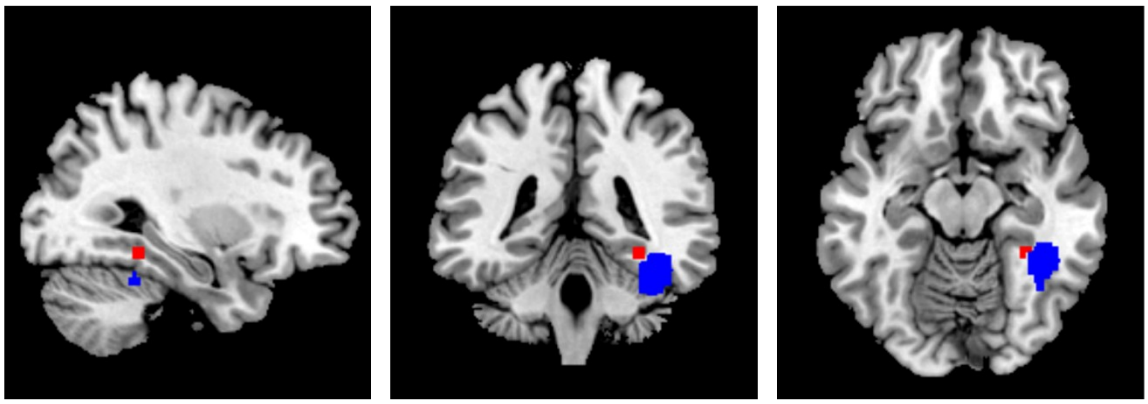

Figure 6. Whole-brain univariate analyses testing for regions showing greater responses to synchronous than asynchronous motion revealed a small cluster (red) with a peak in the right fusiform gyrus [x = 30, y = -40, z = -13]. There was no overlap with the probabilistic map of rFFA (blue) that was used to define our individual FFA ROIs.

It is possible that the activation in right fusiform cortex seen for the contrast synchronous > asynchronous is attributable to rFFA. Note, however, this univariate effect was not seen in the functionally-defined FFA ROIs (Figure 5). To further interrogate this possibility, we examined whether the cluster identified in right fusiform cortex overlapped with the rFFA parcel described by Julian et al. (2012). We observed no overlap – the right fusiform cluster seen in our data was more medial than the rFFA parcel, adjacent to the parahippocampal gyrus (Figure 6).

The functional characteristics of the EBA ROIs

The EBA is thought to show little or no face-selectivity (Peelen & Downing, 2007). The ability of EBA to decode synchronous vs. asynchronous head motion might therefore strike some readers as counter-intuitive. With this in mind, we sought to confirm that our functionally-defined EBA ROIs behaved as expected during the functional localiser procedure. During this procedure, participants viewed dynamic faces, bodies, and objects. Univariate contrasts

were used to define face-selective (faces > objects) and body-selective (bodies > objects) regions.

To examine whether our EBA ROIs showed unexpected face-selectivity, we extracted beta values for faces and objects in rEBA and lEBA and calculated the mean beta value across all voxels included in each ROI, separately for faces and objects. Responses to faces and objects were similar in the rEBA [M_{faces} = 2.346, $M_{objects}$ = 2.481, $t(31) = 1.069$, $p = .293$], and significantly greater for objects in the lEBA [M_{faces} = 1.596, $M_{objects}$ = 1.854, $t(31) = 2.749$, $p = .010$]. This pattern indicates that our functionally-defined EBA ROIs behaved as expected –the EBA ROIs show no selectivity for faces *per se*.

General discussion

The present study employed MVPA to identify visual regions that underlie the perception of interpersonal synchrony/asynchrony. Several regions of the social perception network were found to support significant decoding of synchronous vs. asynchronous head movements, including bilateral EBA, face-selective and interaction-sensitive regions of the mid/posterior rSTS, and rOFA. We saw robust cross-classification in lEBA and rEBA, whereby a classifier trained to discriminate synchronous vs. asynchronous head-shaking, could also discriminate synchronous vs. asynchronous head-nodding, and *vice versa*. Exploratory whole-brain analyses also identified a region of right fusiform cortex that responded more strongly to synchronous than asynchronous motion.

Dedicated processing of social interactions

There is growing suggestion that social interactions may engage specialized visual processing beyond any domain-specific processing of the constituent individuals (Papeo, 2020; Quadflieg & Koldewyn, 2017). In order to isolate interaction-selective processing studies have sought to compare neural responses to dyads shown face-to-face and non-facing; i.e., pairs of individuals shown back-to-back (e.g., Abassi & Papeo, 2020, 2022) or facing the observer (e.g., Centelles et al., 2011). The logic here is that non-facing arrangements contain the same (Abassi & Papeo, 2020, 2022; Bellot et al., 2021) or broadly similar (Centelles et al., 2011; Isik et al., 2017; Kujala et al., 2012; Walbrin et al., 2018) face, body, and action cues to those seen in face-to-face arrangements, but unlike face-to-face arrangements, do not imply social interaction. This approach has repeatedly identified EBA and pSTS as potential sources of interaction processing (Abassi & Papeo, 2020, 2022; Bellot et al., 2021; Centelles et al., 2011; Isik et al., 2017; Kujala et al., 2012; Walbrin et al., 2018).

There is a lingering concern, however, that these effects may reflect attentional modulation of single-actor processing, rather than encoding of interactions *per se* (Vestner, Gray, & Cook, 2020). Faces and bodies viewed in profile cue participants' visuospatial attention (Vestner, Gray, & Cook, 2021). When arranged face-to-face, the directionality of the lefthand actor cues the observer's attention towards the righthand actor, and *vice versa*, creating an 'attention trap'. This is not true of the non-facing conditions. In back-to-back arrangements, for example, the same cues direct observers' attention towards the display periphery. Eye-tracking confirms that participants inspect face-to-face and non-facing dyads differently (Kujala et al., 2012).

Our approach was different: we manipulated interpersonal synchrony without altering the basic dyadic configuration of our stimuli. Because the avatars in our study were always presented face-to-face, decoding of synchrony/asynchrony cannot be attributed to crude differences in arrangement. Critically, the perception of relative-phase requires the extraction and integration of dynamic information from more than one person. Hence, the representation of synchrony/asynchrony cannot be attributed to augmented or additive processing of individuals. Our findings therefore provide crucial new evidence of multi-actor visual processing within the social perception network.

Contribution of EBA and pSTS to interaction perception

We found representations of interpersonal synchrony/asynchrony in bilateral EBA, in an interaction-sensitive rSTS region (STS-I), and in a face-selective rSTS region (STS-F). These results, together with previous findings (Abassi & Papeo, 2020, 2022; Bellot et al., 2021; Centelles et al., 2011; Isik et al., 2017; Kujala et al., 2012; Walbrin et al., 2018; Walbrin & Koldewyn, 2019) suggest that EBA and pSTS may form part of a circuit that underlies the visual perception of social interactions. The STS-I has been shown previously to be more sensitive to social interactions than the adjacent and partially overlapping STS-F region (Isik et al., 2017). However, in our study, synchrony classification accuracy was similar in both pSTS regions.

The emerging body of evidence does not afford a straightforward account of the respective contributions of EBA and pSTS to social interaction perception. Despite its functional selectivity for body stimuli, EBA is thought to show little or no face-selectivity (Peelen & Downing, 2007). Thus, one possibility is that the contribution of EBA to interaction perception is limited to the processing of body cues. At first glance, our findings – obtained with head

and face stimuli – argue against this view. However, the synchronous and asynchronous stimuli used here depicted rigid head movements (nodding or shaking), rather than facial motion *per se* (e.g., O'Toole, Roark, & Abdi, 2002). Thus, while our stimuli are not canonical 'body' stimuli, nor are they canonical 'face' stimuli.

A second possibility is that EBA encodes spatial/temporospatial stimulus features (Quadflieg et al., 2015), whereas pSTS supports further interpretative processing (Centelles et al., 2011). This interpretation is consistent with evidence that EBA is sensitive to the arrangement of actors within dyads (Abassi & Papeo, 2020, 2022), as well as the congruence (Quadflieg et al., 2015) and synchrony (current study) of dyadic interactions. This view also accords with evidence that different types of interaction (e.g., helping vs. hindering) between simple moving shapes (e.g., blue circles, red squares) can be decoded from the responses of STS-I (Isik et al., 2017; Walbrin et al., 2018). Given that the interactions depicted are between simple shapes, these results imply that STS-I represents relatively abstract features of social interactions, and that processing in this region is relatively insensitive to actors' visual appearance / kinematics.

We observed a notable difference between EBA and pSTS in our cross-classification analyses. Representations of synchrony/asynchrony generalised across motion type (nodding and shaking) in bilateral EBA. Interestingly, however, cross-classification did not exceed chance in pSTS. We speculate that responses in pSTS did not support significant cross-classification because head-shaking and head-nodding afford different social interpretations - disagreement and agreement. It is possible that the presence of synchrony affects perceived agreement and disagreement – abstract features potentially encoded within pSTS – but does so differently for nodding and shaking movements.

Univariate analyses of the responses seen in our ROIs revealed that rEBA and lSTS-F responded more strongly to asynchronous head movements than to synchronous head movements. This result mirrors a similar finding reported by Quadflieg et al. (2015) who observed greater activation in EBA and pSTS when participants viewed semantically incongruous face-to-face dyads, relative to congruous dyads. Asynchronous and incongruous dyads may produce stronger univariate responses in these areas because they violate perceptual expectations about the appearance of social interactions and are thus processed inefficiently.

Contribution of other areas

Significant decoding of synchrony/asynchrony in MT is consistent with evidence that MT responds more strongly to videos of dyadic interaction than to videos of people acting independently (Landsiedel et al., 2022), and more strongly to semantically incongruent dyads than to congruent dyads (Quadflieg et al., 2015). The significant decoding seen in MT might reflect the contribution of domain-general motion processing to the perception of interpersonal synchrony (Born & Bradley, 2005). One suggestion is that pSTS and MT are part of a visual pathway for the perception of the actions and movements of others (Pitcher & Ungerleider, 2021).

There is some spatial overlap between MT and EBA (Ferri, Kolster, Jastorff, & Orban, 2013) and the decoding of synchrony/asynchrony seen in MT did not survive the removal of overlapping EBA voxels in our study. In contrast, the decoding seen in EBA remained significant when these voxels were removed from our analyses. It should be noted, however, that the MT region in our study was defined using a probabilistic group map approach which, unlike a functional localizer approach, does not take into account individual variation in the location of MT.

Significant synchrony/asynchrony classification in rOFA is unexpected given that previous studies comparing the processing of congruent and incongruent interactions (Quadflieg et al., 2015) and face-to-face and back-to-back dyads (Abassi & Papeo, 2020) found no difference in OFA activation. Relative to the stimuli used in previous studies, however, our stimuli emphasised the head and face regions. It is thus possible that OFA contributes to the perception of interpersonal synchrony by encoding the relative rotation / orientation of different faces. This feature of our stimuli may also explain the high levels of synchrony/asynchrony decoding seen in STS-F.

Exploratory whole-brain analyses identified an area of right fusiform cortex that showed selectivity for synchronous dyadic motion. Interestingly, there was no sign of this effect in the functionally defined rFFA ROI, nor was there any overlap with the probabilistic map of rFFA derived by Julian et al. (2012). Relative to interpersonal asynchrony, interpersonal synchrony affords grouping (Lakens, 2010; Lakens & Stel, 2011), and attributions of rapport (Lakens & Stel, 2011; Miles et al., 2009). One possibility is that this right fusiform region mediates additional processing engaged selectively by synchronous interactions. It is important that future work elucidates the functional properties of this area; in particular, whether it responds selectively to interpersonal synchrony or to synchrony more generally (e.g., to synchronous interactions between objects, or between people and objects).

Conclusion

Interpersonal synchrony is a critical cue when appraising dynamic social scenes. However, little is known about its neural representation within the human visual system (Cracco et al., 2022). Findings obtained with MVPA indicate that distributed responses throughout the social perception network support categorisation of synchronous vs. asynchronous head movements. Crucially, relative-phase is an emergent property of the actions of multiple actors. These results therefore provide key new evidence of dedicated visual processing of social interactions.

References

Abassi, E., & Papeo, L. (2020). The representation of two-body shapes in the human visual cortex. *Journal of Neuroscience, 40*(4), 852-863.

Abassi, E., & Papeo, L. (2022). Behavioral and neural markers of visual configural processing in social scene perception. *NeuroImage, 260*, e119506.

Bellot, E., Abassi, E., & Papeo, L. (2021). Moving toward versus away from another: How body motion direction changes the representation of bodies and actions in the visual cortex. *Cerebral Cortex, 31*(5), 2670-2685.

Blake, R., & Shiffrar, M. (2007). Perception of human motion. *Annual review of psychology, 58*, 47-73.

Born, R. T., & Bradley, D. C. (2005). Structure and function of visual area MT. *Annual Review of Neuroscience, 28*, 157-189.

Brainard, D. H. (1997). The psychophysics toolbox. *Spatial Vision, 10*(4), 433-436.

Caplovitz, G. P., Barroso, D. J., Hsieh, P. J., & Tse, P. U. (2008). fMRI reveals that non-local processing in ventral retinotopic cortex underlies perceptual grouping by temporal synchrony. *Human Brain Mapping, 29*(6), 651-661.

Centelles, L., Assaiante, C., Nazarian, B., Anton, J. L., & Schmitz, C. (2011). Recruitment of both the mirror and the mentalizing networks when observing social interactions depicted by point-lights: a neuroimaging study. *PloS One, 6*(1), e15749.

Chang, C. C., & Lin, C. J. (2011). LIBSVM: a library for support vector machines. *ACM transactions on intelligent systems and technology (TIST), 2*(3), 1-27.

Cracco, E., Lee, H., van Belle, G., Quenon, L., Haggard, P., Rossion, B., & Orgs, G. (2022). EEG frequency tagging reveals the integration of form and motion cues into the perception of group movement. *Cerebral Cortex, 32*(13), 2843-2857.

Duchaine, B., & Yovel, G. (2015). A revised neural framework for face processing. *Annual Review of Vision Science, 1*, 393-416.

Fedorenko, E., Hsieh, P. J., Nieto-Castañón, A., Whitfield-Gabrieli, S., & Kanwisher, N. (2010). New method for fMRI investigations of language: defining ROIs functionally in individual subjects. *Journal of Neurophysiology, 104*(2), 1177-1194.

Ferber, S., Humphrey, G. K., & Vilis, T. (2003). The lateral occipital complex subserves the perceptual persistence of motion-defined groupings. *Cerebral Cortex, 13*(7), 716-721.

Ferri, S., Kolster, H., Jastorff, J., & Orban, G. A. (2013). The overlap of the EBA and the MT/V5 cluster. *NeuroImage, 66*, 412-425.

Haxby, J. V., Hoffman, E. A., & Gobbini, M. I. (2000). The distributed human neural system for face perception. *Trends in Cognitive Sciences, 4*, 223-233.

Hebart, M. N., Görgen, K., & Haynes, J. D. (2015). The Decoding Toolbox (TDT): a versatile software package for multivariate analyses of functional imaging data. *Frontiers in Neuroinformatics, 8*, e88.

Hoehl, S., Fairhurst, M., & Schirmer, A. (2021). Interactional synchrony: signals, mechanisms and benefits. *Social Cognitive and Affective Neuroscience, 16*, 5-18.

Isik, L., Koldewyn, K., Beeler, D., & Kanwisher, N. (2017). Perceiving social interactions in the posterior superior temporal sulcus. *Proceedings of the National Academy of Sciences, 114*(43), E9145-E9152.

Julian, J. B., Fedorenko, E., Webster, J., & Kanwisher, N. (2012). An algorithmic method for functionally defining regions of interest in the ventral visual pathway. *NeuroImage, 60*(4), 2357-2364.

Kolster, H., Peeters, R., & Orban, G. A. (2010). The retinotopic organization of the human middle temporal area MT/V5 and its cortical neighbors. *Journal of Neuroscience, 30*(29), 9801-9820.

Kujala, M. V., Carlson, S., & Hari, R. (2012). Engagement of amygdala in third-person view of face-to-face interaction. *Human Brain Mapping, 33*(8), 1753-1762.

Lakens, D. (2010). Movement synchrony and perceived entitativity. *Journal of experimental social psychology, 46*(5), 701-708.

Lakens, D., & Stel, M. (2011). If they move in sync, they must feel in sync: Movement synchrony leads to attributions of rapport and entitativity. *Social Cognition, 29*(1), 1-14.

Landsiedel, J., Daughters, K., Downing, P. E., & Koldewyn, K. (2022). The role of motion in the neural representation of social interactions in the posterior temporal cortex. *NeuroImage, 262*, e119533.

Latif, N., Barbosa, A. V., Vatiokiotis-Bateson, E., Castelhano, M. S., & Munhall, K. G. (2014). Movement coordination during conversation. *PloS One, 9*(8), e105036.

Marsh, K. L., Richardson, M. J., & Schmidt, R. C. (2009). Social connection through joint action and interpersonal coordination. *Topics in Cognitive Science, 1*(2), 320-339.

Miles, L. K., Nind, L. K., & Macrae, C. N. (2009). The rhythm of rapport: Interpersonal synchrony and social perception. *Journal of experimental social psychology, 45*(3), 585-589.

O'Toole, A. J., Roark, D. A., & Abdi, H. (2002). Recognizing moving faces: A psychological and neural synthesis. *Trends in Cognitive Sciences, 6*(6), 261-266.

Papeo, L. (2020). Twos in human visual perception. *Cortex, 132*, 473-478.

Peelen, M. V., & Downing, P. E. (2007). The neural basis of visual body perception. *Nature Reviews Neuroscience, 8*(8), 636-648.

Pelli, D. G. (1997). The VideoToolbox software for visual psychophysics: transforming numbers into movies. *Spatial Vision, 10*(4), 437-442.

Pitcher, D., Dilks, D. D., Saxe, R. R., Triantafyllou, C., & Kanwisher, N. (2011). Differential selectivity for dynamic versus static information in face-selective cortical regions. *NeuroImage, 56*(4), 2356-2363.

Pitcher, D., & Ungerleider, L. G. (2021). Evidence for a third visual pathway specialized for social perception. *Trends in Cognitive Sciences, 25*(2), 100-110.

Quadflieg, S., Gentile, F., & Rossion, B. (2015). The neural basis of perceiving person interactions. *Cortex, 70*, 5-20.

Quadflieg, S., & Koldewyn, K. (2017). The neuroscience of people watching: how the human brain makes sense of other people's encounters. *Annals of the New York Academy of Sciences, 1396*(1), 166-182.

Rolls, E. T., Huang, C. C., Lin, C. P., Feng, J., & Joliot, M. (2020). Automated Anatomical Labelling Atlas 3. *NeuroImage, 206*, e116189.

Stelzer, J., Chen, Y., & Turner, R. (2013). Statistical inference and multiple testing correction in classification-based multi-voxel pattern analysis (MVPA): random permutations and cluster size control. *NeuroImage, 65*, 69-82.

Vestner, T., Gray, K. L., & Cook, R. (2020). Why are social interactions found quickly in visual search tasks? *Cognition, 200*, e104270.

Vestner, T., Gray, K. L., & Cook, R. (2021). Visual search for facing and non-facing people: The effect of actor inversion. *Cognition, 208*, e104550.

Walbrin, J., Downing, P., & Koldewyn, K. (2018). Neural responses to visually observed social interactions. *Neuropsychologia, 112*, 31-39.

Walbrin, J., & Koldewyn, K. (2019). Dyadic interaction processing in the posterior temporal cortex. *NeuroImage, 198*, 296-302.

Wang, L., Mruczek, R. E., Arcaro, M. J., & Kastner, S. (2015). Probabilistic maps of visual topography in human cortex. *Cerebral Cortex, 25*(10), 3911-3931.